Proceedings of the 7th International Conference on Asian and Pacific Coasts (APAC 2013) Bali, Indonesia, September 24-26, 2013

WAVE HINDCAST FROM INTEGRALLY COUPLED WAVE-TIDE-SURGE MODEL OF THE EAST CHINA SEA

K. O. Kim [1], B. H. Choi [2] and J. H. Yuk [3]

ABSTRACT: With the recent introduction of the coupled system (ADCIRC hydrodynamic and SWAN wave model) which can run on the same unstructured mesh, allowing the physics of wave-circulation interactions to be correctly resolved in both models and all energy from deep to shallow waters to be seamlessly followed, the resulting modeling system can be used extensively for the prediction of typhoon surges and usual barotropic forecast. The result confirms the necessity to incorporate the wave-current interaction effect into coastal area in the wave-tide-surge coupled model. At the same time, effects of depth-induced wave breaking, wind field, currents and sea surface elevation in prediction of waves are included. Especially, we found that the wind wave significantly enhances the current and surge elevation. The resulting modeling system can be used for hindcasting (prediction) and forecasting the wave-tide-surge distribution in the environments with complex coastline, shallow water and fine sediment area like around Korean Peninsula.

Keywords: Coupled wave-tide-surge model, unstructured mesh, the East China Sea

INTRODUCTION

The recent introduction of unstructured wave models has made nesting unnecessary and the coupled system (unstructured-mesh SWAN wave and ADCIRC) can run on the same unstructured mesh. This identical and homogeneous mesh allows the physics of wave-circulation interactions to be correctly resolved in both models. The unstructured mesh can be applied to a large domain allowing all energy from deep to shallow waters to be seamlessly followed. There is no nesting or overlapping of structured wave meshes, and no interpolation is required. The problem of wave reflection in the nesting boundary for the uncompleted feedback to mother's domain can be avoided. The waves and storm surge are allowed to develop on the continental shelf and interact with the complex nearshore environment.

In this study the integrally coupled wave-tide-surge model has been developed and then applied to the simulation of wave-typhoon surge for typhoon Sarah (5914) which destroyed Korean and Japanese coasts extensively in 1959. Modeling methods and results are presented and discussed in terms of the effect of tide-surge-wave interaction.

NUMERICAL MODEL

Wave Model

SWAN (Simulating WAves Nearshore) predicts the evolution in geographical space and time of the wave action density spectrum, with the relative frequency (σ) and the wave direction (θ), as governed by the action balance equation (Booij et al. 1999):

$$\frac{\partial N}{\partial t}+\nabla_{\vec{x}}\left[\left(\vec{c}_g+\vec{U}\right)N\right]+\frac{\partial c_\theta N}{\partial \theta}+\frac{\partial c_\sigma N}{\partial \sigma}=\frac{S_{tot}}{\sigma} \quad (1)$$

where the terms on the left-hand side represent, respectively, the change of wave action in time, t, the propagation of wave action in space (with $\nabla_{\vec{x}}$ the gradient operator in geographic space, the $\vec{c}_g$ wave group velocity and $\vec{U}$ the ambient current vector), depth and current induced refraction and approximate diffraction (with propagation velocity or turning rate c_θ), and the shifting of wave action due to variations in mean current and depth (with propagation velocity or shifting rate c_σ). The source term, S_{tot}, represents wave growth by wind; action lost due to whitecapping, surf breaking and bottom friction and action exchanged between spectral components in deep and shallow water due to nonlinear effects. The associated SWAN parameterizations are given by Booij et al. (1999), with all subsequent modifications as present in version 40.72, including the phase-decoupled refraction–diffraction (Holthuijsen et al. 2003), although diffraction is not enabled in the present simulations. The unstructured-mesh version of SWAN implements an analog to the four-direction Gauss–Seidel iteration technique employed in the structured version, and it maintains SWAN's unconditional stability (Zijlema 2010). SWAN

[1] Marine Environments & Conservation Research Division, Korea Ins. of Ocean Science & Technology, Ansan, 426-744, KOREA
[2] Department of Civil and Environmental Engineering, Sungkyunkwan University, Suwon, 440-746, KOREA
[3] Supercomputing Center, Korea Institute of Science and Technology Information, Daejeon, 305-806, KOREA

computes the wave action density spectrum at the vertices of an unstructured triangular mesh, and it orders the mesh vertices so it can sweep through them and update the action density using information from neighboring vertices.

Tide and Surge Model

ADCIRC (the ADvanced CIRCulation model) is a continuous-Galerkin, finite-element, shallow-water model that solves for water levels and currents at a range of scales (Westerink et al. 2008; Luettich and Westerink 2004; Atkinson et al. 2004; Dawson et al. 2006). The details of this solution have been published widely (http://www.nd.edu/~adcirc/manual.htm to see Users Manual and Theory Report) and will not be stated here.

Sharing Information

SWAN is driven by wind speeds, water levels and currents computed at the vertices by ADCIRC. Marine winds can be input to ADCIRC in a variety of formats, and these winds are adjusted directionally to account for surface roughness (Bunya et al. 2010). ADCIRC uses spatial and temporal interpolations to project these winds to the computational vertices, and then it passes them to SWAN. The water levels and ambient currents are computed in ADCIRC before being passed to SWAN, where they are used to recalculate the water depth and all related wave processes (wave propagation, depth-induced breaking, etc.). The ADCIRC model is driven partly by radiation stress gradients that are computed using information from SWAN. These gradients, τ_s , waves are computed by:

$$\tau_{sx,wave} = -\frac{\partial S_{xx}}{\partial x} - \frac{\partial S_{xy}}{\partial y} \tag{2}$$

$$\tau_{sy,wave} = -\frac{\partial S_{xy}}{\partial x} - \frac{\partial S_{yy}}{\partial y} \tag{3}$$

where S_{xx}, S_{xy} and S_{yy} are the wave radiation stresses (Longuet–Higgins and Stewart 1964; Battjes 1972).

ADCIRC and SWAN run in series on the same local mesh and core. The two models "leap frog" through time, each being forced with information from the other model. To update the wave information at the computational vertices in SWAN takes much larger time steps than ADCIRC, which is diffusion- and also Courant time step-limited due to its semi-explicit formulation and its wetting and drying algorithm. For that reason, the coupling interval is taken to be the same as the time step of SWAN. On each coupling interval, ADCIRC run first, because the nearshore and the coastal floodplain, wave properties are assumedly more dependent on circulation. At the beginning of each coupling interval, ADCIRC accesses the radiation stress gradients computed by SWAN at times corresponding to the beginning and end of the previous interval. ADCIRC uses that information to extrapolate the gradients at all of its time steps in the current interval. These extrapolated gradients are then used to force the ADCIRC solution as described previously. Once the ADCIRC stage is completed, SWAN runs for one time step, to bring it to the same moment in time as ADCIRC. SWAN can access the wind speeds, water levels and currents computed at the mesh vertices by ADCIRC, at times corresponding to the beginning and end of the current interval. SWAN applies the mean of those values to force its solution at its time step. In this way, the radiation stress gradients used by ADCIRC are always extrapolated forward in time, while the wind speeds, water levels and currents used by SWAN are always averaged over each of its time steps. The basic structure of this coupling system (ADCIRC+SWAN) was developed by Dietrich et al. (2010). A schematic of the communication is shown in Fig. 1.

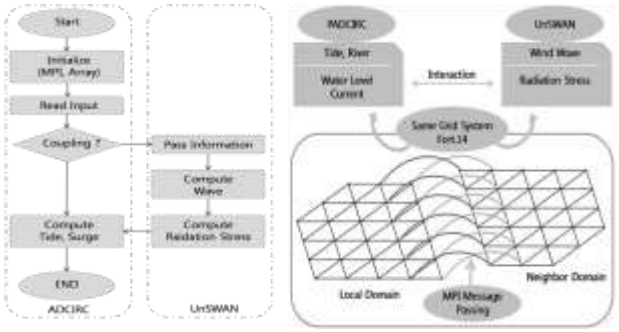

Fig. 1 Schematic of parallel communication between models and cores. Solid lines indicate communication for the edge-layer-based nodes between sub-meshes, and are intra-model and inter-core (Choi et al. 2013)

MODEL SETUPS FOR TYPHOON SARAH (5914)

Meteorological Forcing Input

For the simulation, Grid Point Values (GPVs) of sea level pressure and air and sea surface temperatures with 50 km intervals over the Northeast Asian seas were digitized by Japan Weather Association (JWA). Those values were interpolated to dense 1/12° grid resolution at one hourly interval from six hourly dataset for the coupled model. The overall marine wind fields are computed by adopting Planetary Marine Boundary Layer model (Cardone 1969) and then the typhoon model winds by Rankin vortex model (Fujita 1952) were inserted. Temporal interpolation along the typhoon track was also performed.

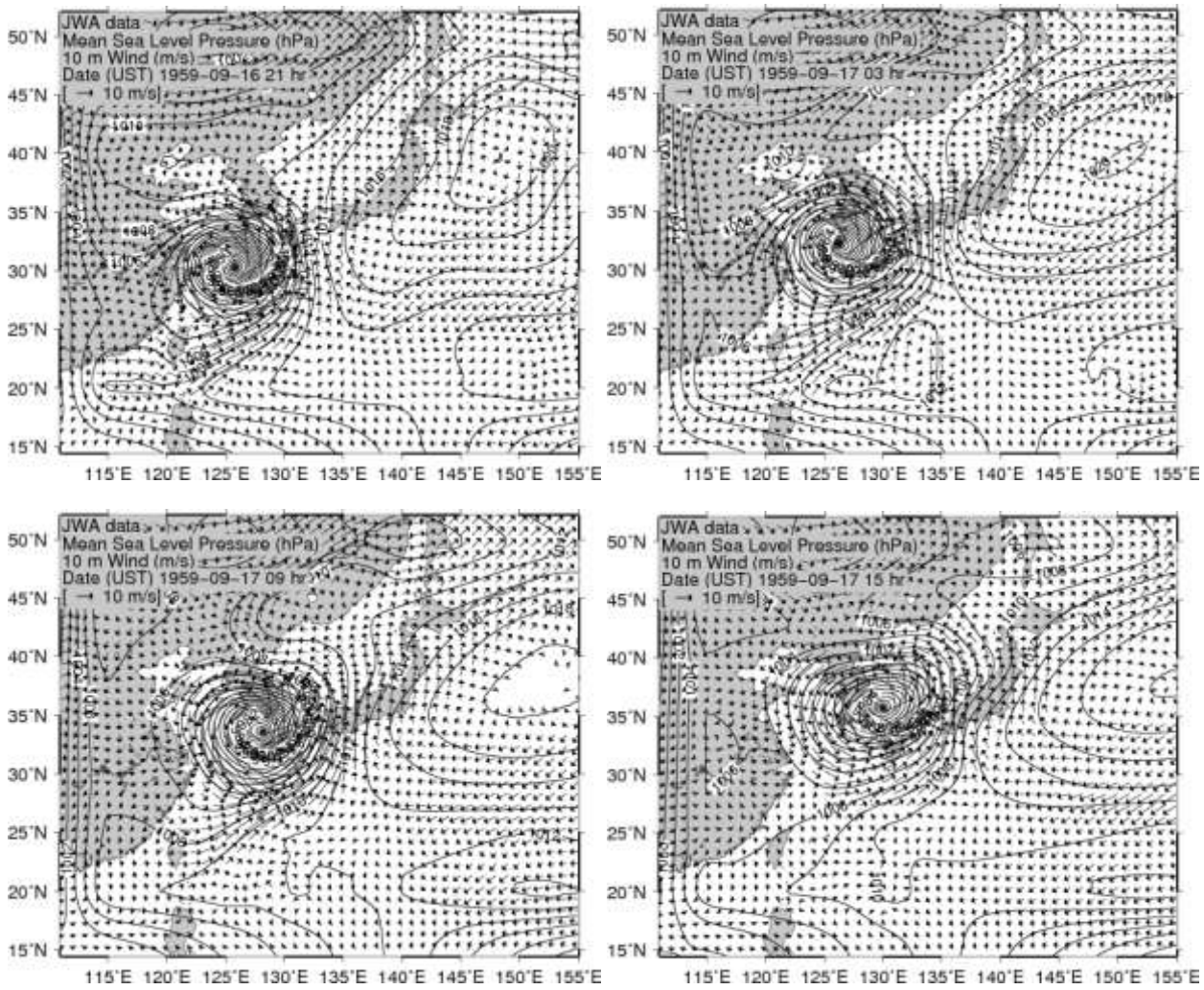

Fig. 2 Distribution of wind and pressure fields for the typhoon Sarah (5914)

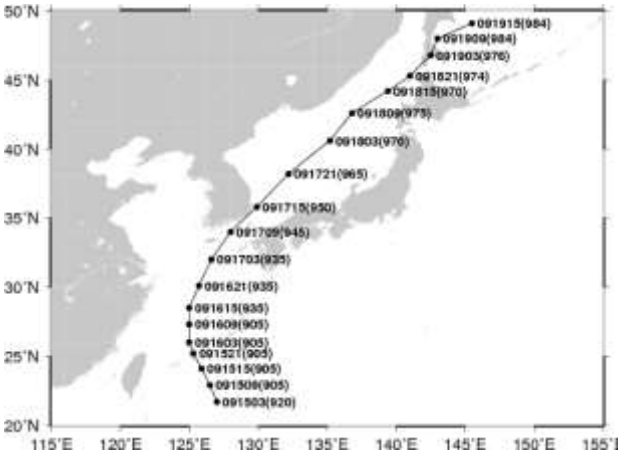

Fig. 3 Track of the typhoon Sarah (5914). The numbers in the parenthesis indicates the typhoon center pressure (hPa).

Fig. 2 shows the computed results of pressure and wind vector fields for the typhoon Sarah (5914) at the interval of 6 hr from 21:00 UST Sep. 16. The track of the typhoon Sarah (5914) selected for the simulation is shown in Fig. 3. Typhoon Sarah (5914) formed in September off the coast of Saipan and tracked northwestward with a pressure of 905 hPa and winds up to 65 m/s over northeastern Taiwan at a speed of about 25 km/h. Typhoon Sarah then moved north-northeastward with a pressure of 945 hPa passing south of Korean Peninsula, resulting in a death and missing toll of 849 with 2533 people injured.

Model Parameters

The complex mesh resolutions are shown in Fig. 4. This mesh incorporated local resolution down to 50 m, and covered the Yellow, East Seas and the western Pacific Ocean, including hundreds of islands, with the sufficient resolution of the wave-transformation zones near the coasts and intricate representation of various natural and man-made geographic features. A total of 208,416 vertices and 383,715 triangular elements were contained in the mesh.

Open boundary forcing was applied in the form of specifications based on NAO's (National Astronomical Observatory) tidal predictions (Matsumoto et al. 2000) along the model's open water boundary. The sea level pressures and wind field, which were predicted by JWA data mentioned above. The SWAN time step and the coupling interval were set to 300 sec. The version of SWAN 40.85 was used with default settings in the simulation.

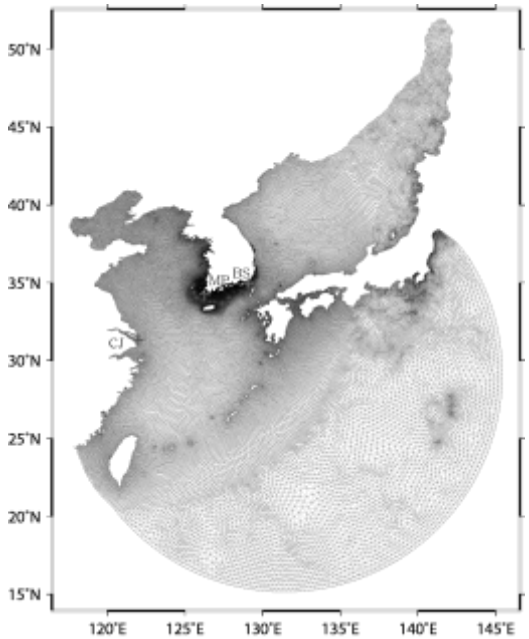

Fig. 4 Mesh system of model. CJ: Mouth of Changjiang River, MP: Mokpo, BS: Busan

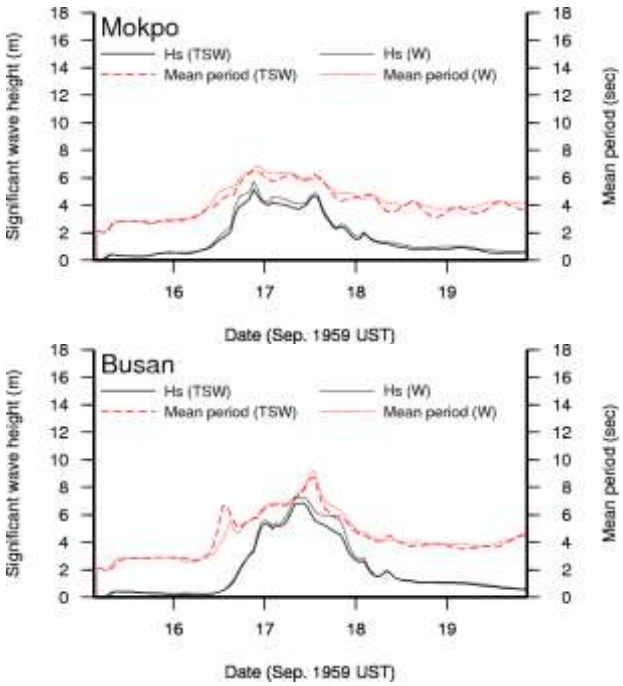

Fig. 5 Comparisons of Hs and mean period computed by coupled tide-surge-wave model (TSW; thick lines) and wave model (W; thin lines)

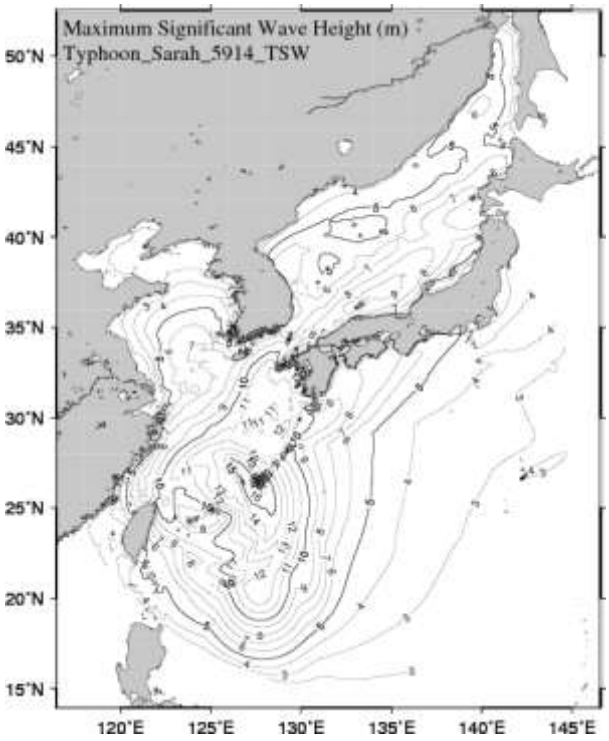

(a) Coupled tide-surge-wave (TSW) model

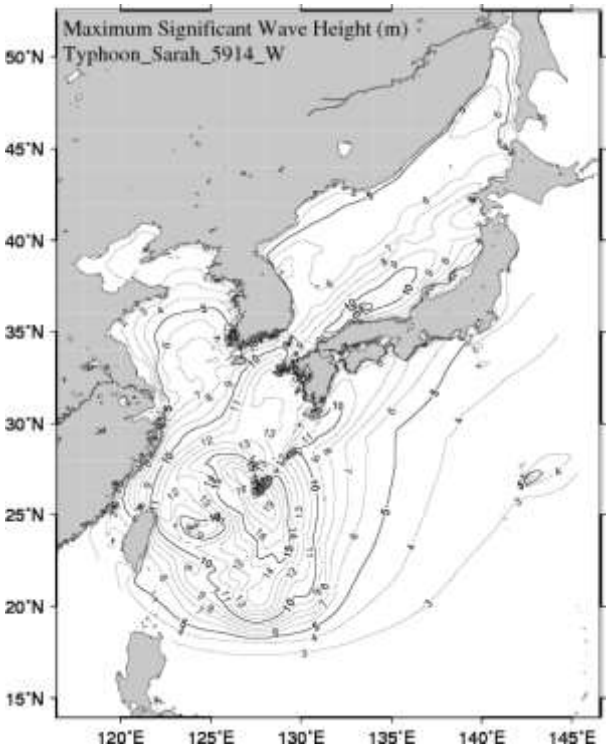

(b) Wave (W) model

Fig. 6 Distribution of maximum significant wave height in the model domain

MODEL RESULTS

Validation of typhoon Sarah (5914) case is not carried out because this event occurred in the very past year, 1959, and there were no observation. However this

integrally coupled wave-tide-surge model was used and reproduced the reasonable results for typhoon Maemi (2003) case (Choi et al. 2013).

We extract the time series of significant wave height (Hs) and mean period computed by the coupled tide-surge-wave (TSW) model and wave (W) model in Busan and Mokpo during the typhoon event (Fig. 5). The maximum significant wave height is about 7 m in Busan and the significant wave height in Mokpo exceeds about 5 m. These results are similar to the previous study based on WAM (WAMDI Group, 1988) (Choi et al. 2003). The significant wave height computed by TSW model is a little bit less than that computed by W model during the typhoon passage.

Fig. 6 and 7 show the distribution of maximum significant wave height simulated by TSW and W model in the overall model domain and the south coast of Korea including Busan. The highest values are computed as 5 ~ 9 m, 5 m and 7 ~ 11 m along the track of typhoon around the south coasts of Korea, the Changjiang River in China, and the west coasts of Japan, respectively. The significant wave height is the highest as about 16 m in Naha, Japan which is located in the right of typhoon with the lowest center pressure of 905 hPa.

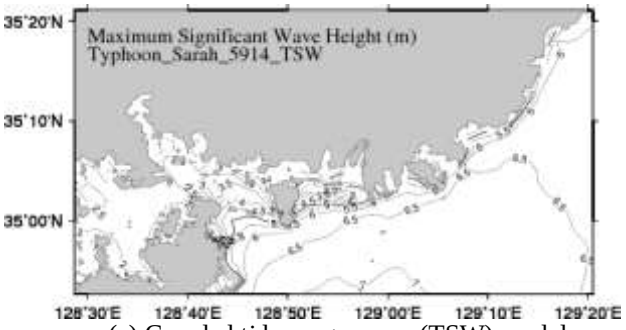

(a) Coupled tide-surge-wave (TSW) model

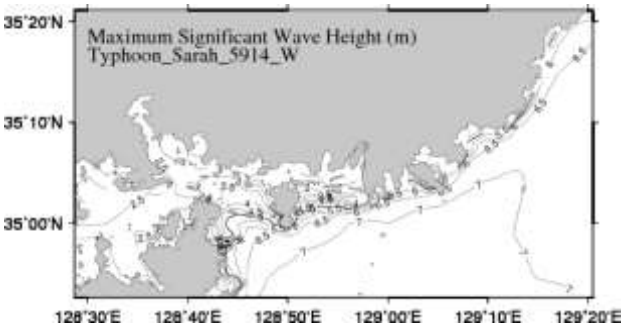

(b) Wave (W) model

Fig. 7 Distribution of maximum significant wave height in the south coast of Korea

The pattern of contours of the wave (W) model is similar to the result of the coupled tide-surge-wave (TSW) model, but in general the value is larger than the TSW model result (Fig. 6a and 7a). The difference between two model results is the highest with about 3 m near Naha, Japan and is about 0.5 m in the south coast of Korea including Busan. We calculated the difference of significant wave height between TSW and W models to understand the effect of tide-surge-wave interaction, and Fig. 8 displays the negative maximum of difference by subtract the significant wave height of W from TSW model. The negative maximum ranges from -3.5 to 0 m and from -2 to 0 m in the East China Sea and the East (Japan) Sea, respectively. In the south coast of Korea, the negative maximum of difference of significant wave height ranged from -1 to 0.5 m. On the other hand, the positive maximum is very small compared with the negative maximum difference, and the values are about 0 and 0.2 m in the East (Japan) Sea and the East China Sea, respectively.

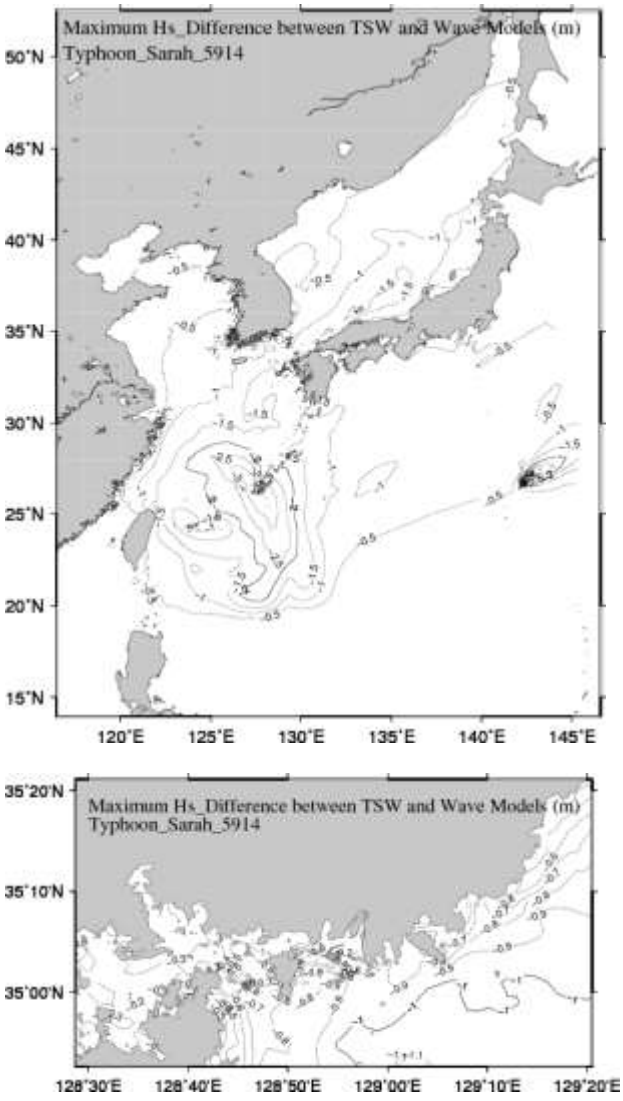

Fig. 8 Negative maximum of difference (TSW-W) of the significant wave height between TSW and W models

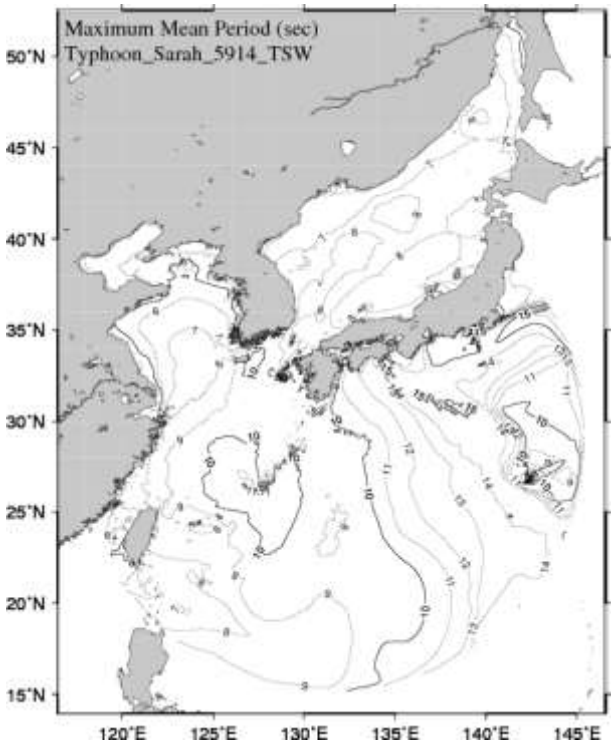

(a) Coupled tide-surge-wave (TSW) model

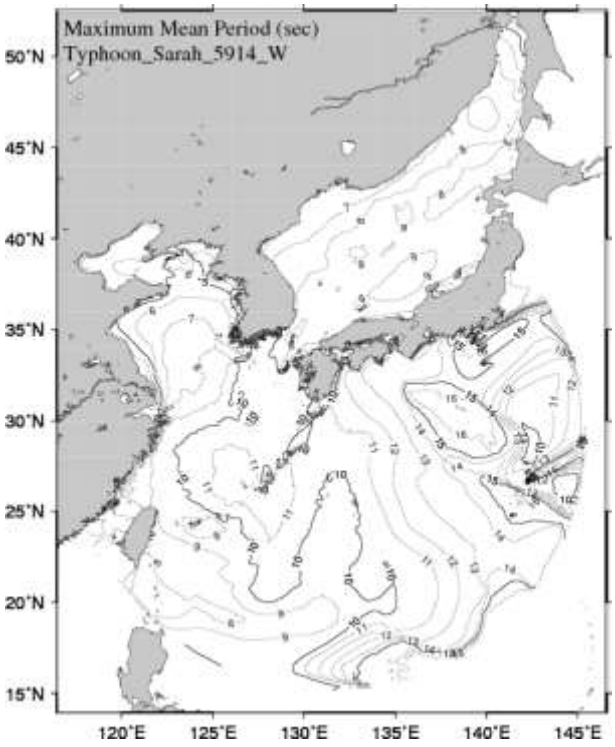

(b) Wave (W) model

Fig. 9 Distribution of maximum mean period (TM01) in the model domain

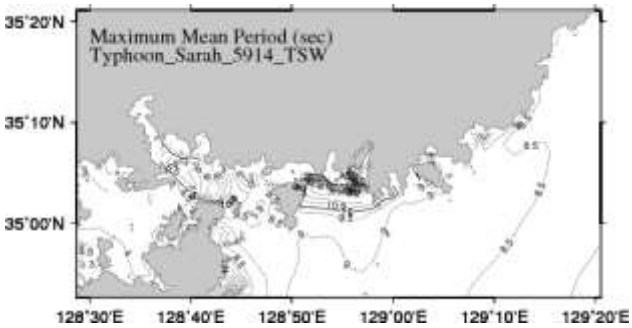

(a) Coupled tide-surge-wave (TSW) model

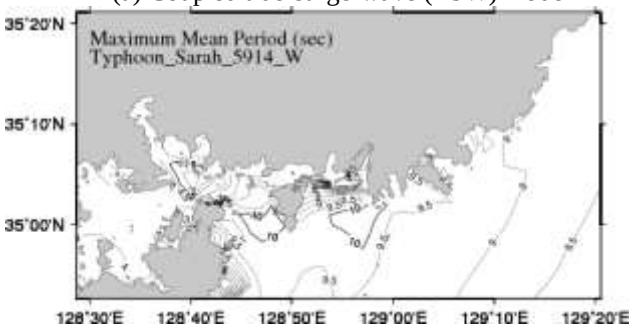

(b) Wave (W) model

Fig. 10 Distribution of maximum mean period (TM01) in the south coast of Korea

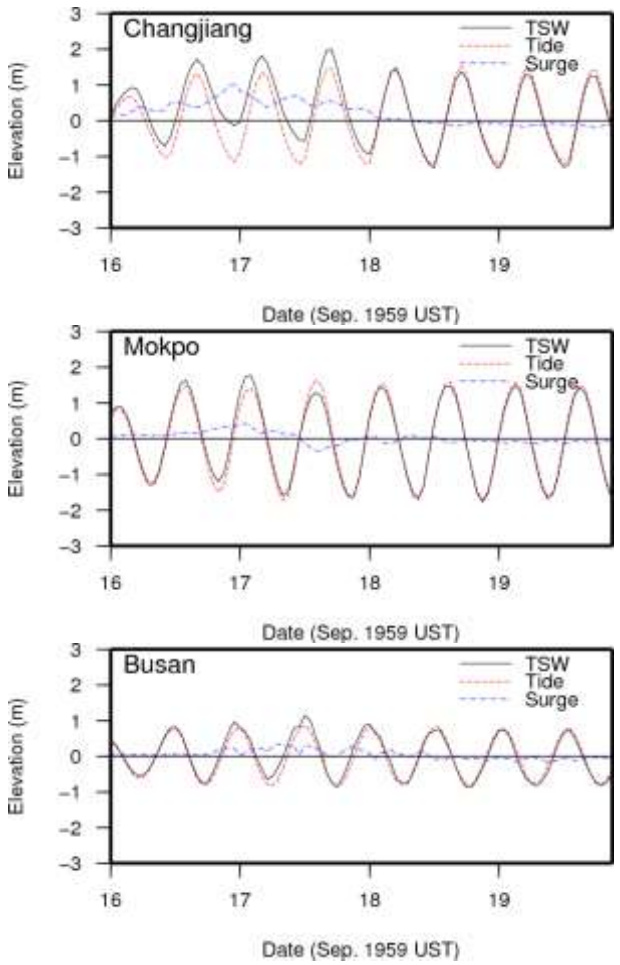

Fig. 11 Time series of water elevation relative to tide level in Changjiang River, Mokpo and Busan

Maximum mean period is also calculated by two models and compared in the overall model domain (Fig. 9) and the south coast of Korea (Fig. 10). Fig. 9 shows the distribution of maximum mean period in the same regions as Fig. 6, and the mean periods are 6 ~ 9, over 10, 8 ~ 11 and 7 ~ 8 sec around the west coasts of Korea, near the mouth of Changjiang River, the south coast of Korea and the East (Japan) Sea, respectively. In general, the wave period computed by the wave model is longer than that of the coupled tide-surge-wave model throughout the model domain.

Fig. 11 shows time series of water elevations in the mouth of Changjiang River, Mokpo and Busan. The surge elevation reached about 1 m in the mouth of Changjiang River around 00:00 UST Sep. 17 and the highest surge elevation was 0.5 m in Mokpo and Busan during typhoon Sarah. The surge elevation is in the range of -0.2 ~ -1 m, -0.2 ~ 0.5 m and -0.2 ~ 0.5 m in the mouth of Changjiang River, Mokpo and Busan, respectively.

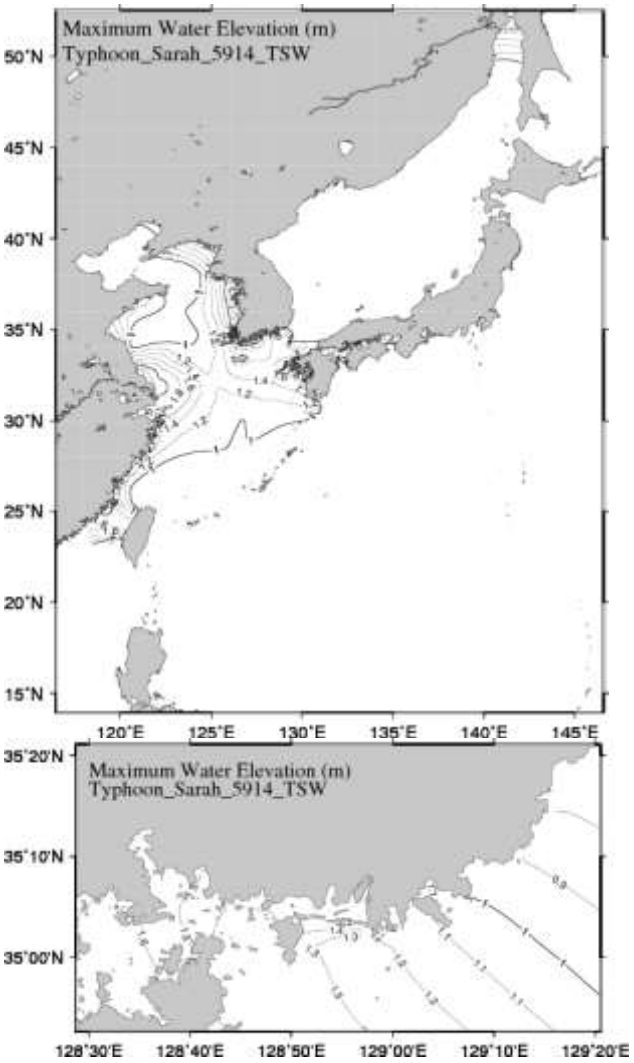

Fig. 12 Distribution of maximum water elevation computed by the TSW model

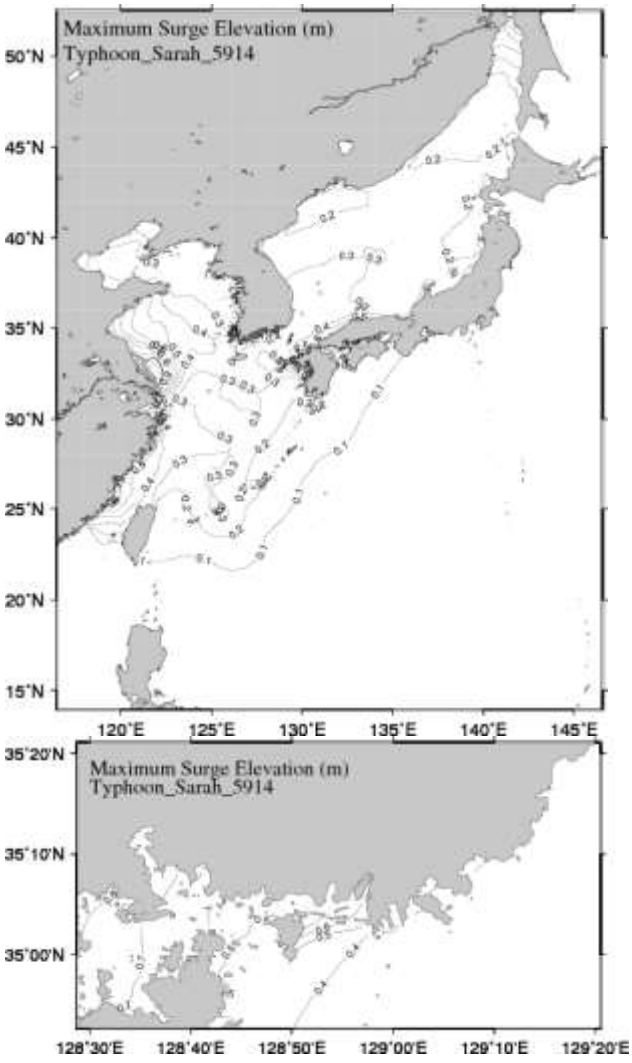

Fig. 13 Distribution of maximum surge elevation

The distribution of maximum water elevation computed by the TSW model is shown in Fig. 12. The maximum water elevation is in the range of 0.8 ~ 1.7 m in the south coast of Korea. Fig. 13 shows the distribution of maximum surge elevation during typhoon Sarah. The highest surge elevation is near the mouth of Changjinag River, and the surge elevation exceeds 1.5 m. The surge elevation is averagely about 0.3 m in the East China Sea and the East (Japan) Sea, and in the range of 0.4 ~ 0.8 m in the south coast of Korea.

CONCLUSIONS

The integrally coupled wave-tide-surge system was developed based on the unstructured mesh sharing the wave and tide-surge models. The numerical model using the structured grid is required to involve the nesting, overlapping and interpolation. The simulation of typhoon Sarah using the coupled model shows reasonable results comparing with the previous researches. In this study, one experiment of the wave hindcast for the East China Sea is presented, however

more experiments for the past events such typhoons and winter monsoons will be conducted with refining the mesh and water depth to resolve the regions of interest.

ACKNOWLEDGEMENTS

The study was supported by the project for the development of the marine environmental impact prediction system following the disastrous events funded by KIOST. The simulation was performed at the Supercomputing Center at Korea Institute of Science and Technology Information (KISTI).

REFERENCES

Atkinson, J.H., Westerink, J.J. and Hervouet, J.M. (2004). Similarities between the wave equation and the quasi-bubble solutions to the shallow water equations. International Journal for Numerical Methods in Fluids 45:689-714.

Battjes, J.A. (1972). Radiation stresses in short-crested waves. Journal of Marine Research, 30(1): 56-64.

Booij, N., Ris, R.C. and Holthuijsen, L.H. (1999). A third-generation wave model for coastal regions, Part I, Model description and validation. J. Geoph. Research, 104: 7649-7666.

Bunya, S. and Coauthors (2010). A high-resolution coupled riverine flow, tide, wind, wind wave, and storm surge model for southern Louisiana and Mississippi. Part I: Model development and validation. Mon. Wea. Rev., 138: 345–377.

Cardone, V. J. (1969). Specification of the wind distribution in the marine boundary layer for wave forecasting. Tech. Rep. 69-1, Geophysical Sciences Laboratory, New York University, 131 pp.

Choi, B.H., Eum, H.M. and Woo, S.B. (2003). Modeling of coupled tide-wave-surge process in the Yellow Sea. Ocean Engineering, 30:739-759.

Choi, B.H., Min, B.I., Kim, K.O. and Yuk, J.H. (2013). Wave-tide-surge coupled simulation for typhoon Maemi. China Ocean Engineering, 27(2):141-158.

Dawson, C., Westerink, J.J., Feyen, J.C. and Pothina, D. (2006). Continuous, discontinuous and coupled discontinuous continuous Galerkin finite element methods for the shallow water equations. Int. J. Numer. Methods Fluids, 52:63-88.

Dietrich, J.C., Bunya, S., Westerink, J.J., Ebersole, B.A., Smith, J.M., Atkinson, J.H., Jensen, R., Resio, D.T., Luettich, R.A., Dawson, C., Cardone, V.J., Cox, A.T., Powell, M.D., Westerink, H.J. and Roberts, H.J. (2010). A high-resolution coupled riverine flow, tide, wind, wind wave and storm surge model for southern Louisiana and Mississippi, Part II: Synoptic description and analyses of Hurricanes Katrina and Rita, Monthly Weather Review, 138:378-404.

Fujita, T. (1952). Pressure distribution within typhoon. Geophysics Magazine 23:437-451.

Holthuijsen, L.H., Herman, A. and Booij, N. (2003). Phase-decoupled refraction - diffraction for spectral wave models, Coast. Eng., 49(4):291-305.

Longuet-Higgins, M.S. and Stewart, R.W. (1964). Radiation stresses in water waves; physical discussions, with applications. Deep Sea Research and Oceanographic Abstracts, 11(4):529-562.

Luettich, R.A., and J. J. Westerink, J.J. (2004). Formulation and numerical implementation of the 2D/3D ADCIRC finite element model version 44.XX, 74 pp.

Matsumoto, K., Takanezawa, T. and Ooe, M. (2000). Ocean tide models developed by assimilating TOPEX/POSEIDON altimeter data into hydrodynamical model: A global model and a regional model around Japan, Journal of Oceanography, 56(5):567-581.

WAMDI Group (1988). The WAM model—a third generation ocean wave prediction model. Journal of Physical Oceanography 18:1775-1810.

Westerink, J.J. and Coauthors (2008). A basin- to channel-scale unstructured grid hurricane storm surge model applied to southern Louisiana. Mon. Wea. Rev., 136:833-864.

Zijlema, M. (2010). Computation of wind-wave spectra in coastal waters with SWAN on unstructured grids. Coast. Eng., 57(3):267-277.